Journal of Materials Chemistry

Cite this: *J. Mater. Chem.*, 2011, **21**, 17798

www.rsc.org/materials

**PAPER**

# Substituent effect on the electronic properties of pyrazino[2,3-*g*] quinoxaline molecules†

**Teck Lip Tam,[ab] Feng Zhou,[ab] Hairong Li,[ab] Jane Chieh Yu Pang,[ab] Yeng Ming Lam,[ab] Subodh G. Mhaisalkar,[ab] Haibin Su*[ab] and Andrew C. Grimsdale*[ab]**

***Received 26th May 2011, Accepted 8th September 2011***
**DOI: 10.1039/c1jm12347e**

We report the synthesis and characterization of pyrazino[2,3-*g*]quinoxaline derivatives with a systematic change in the substituents at the 2, 3, 7 and 8 positions and with or without 2-thienyl at the 5 and 10 positions to study the substituent effect and quinoid character of such a system. We performed density functional theory calculations using the B3LYP functional and 6-31G* basis set under the geometry optimization condition, together with the resonance effect of a valence bond theory to understand the electronic structures of these molecules. It was found that a combination of conjugation and cross-conjugation effects is responsible for the observed trends in their electronic properties, thus giving insights into designing molecules utilizing such effects.



## Introduction

To date, the donor–acceptor (D–A) approach utilizing intramolecular charge-transfer between donor and acceptor units, and a planarization approach *via* quinoidization of a conjugated system are the two main approaches to achieve low band gap materials.[1] The former is in molecular-orbital theory, a consequence of hybridization of energy levels of donor and acceptor moieties.[2,3] The latter is a result of dearomatization of the conjugated backbone *via* quinoid formation, by incorporation of an aromatic system with higher resonance energy.[1] The pyrazino[2,3-*g*]quinoxaline (PQ) system is thus a good candidate acceptor unit for low band gap materials due to its strong electron accepting ability and high quinoid character at 5 and 10 positions.[4–8] The strong π–π interactions between the PQ moieties also make them highly crystalline in nature which is desirable for promoting efficient exciton migration and high charge carrier mobility.[4,9–13] These intrinsic properties of PQ thus make it a good candidate for the development of low band gap and high mobility materials for[1] organic photovoltaics (OPVs).[4,8,11,14–16] Varying substituents at the different positions of PQ using appropriate synthetic routes, allows the study of substituent effects on the overall electronic properties. Here, we report the synthesis and characterization of a series of PQ molecules with a systematic change in the substituents at various positions. Together with computational modeling using density functional theory (DFT)[18] and valence bond theory (VBT), a study of substituent effects on the electronic properties of these complex systems was carried out.

## Results and discussion

### Synthesis

Synthesis of PQ units can be easily carried out by condensation of 1,2-diketones with 1,2,4,5-tetraaminobenzene tetrahydrochloride (TAB). Using different substituted 1,2-diketones, the 2, 3, 7 and 8 positions (arm positions) of PQ can be functionalized with various groups.[9–11,15,19] For PQ substituted at the 5 and 10 positions (quinoidal positions), the required synthetic approach is more complex. It requires reduction of 5,6-dinitro-2,1,3-benzothiadiazole derivatives using zinc and acetic acid, followed by addition of 1,2-diketones.[14,16] In a previous paper, we have demonstrated the use of 4,8-disubstituted benzobisthiadiazole (BBT) as a synthetic equivalent to 4,7-disubstituted-5,6-dinitro-2,1,3-benzothiadiazole for the synthesis of 5,10-disubstituted PQ derivatives.[17,20] In this paper, we expand this approach and introduce four new PQ molecules with biphenyl and/or bithienyl arms, with or without thienyl substitutions at the quinoidal positions to perform a systematic study of the effects of substitution at these positions (Fig. 1).

The synthesis of **PQ-1A** and **PQ-3A** involves the condensation of **TAB** with 1,2-diketones in acetic acid under reflux conditions (Scheme 1). It was found that addition of a catalytic amount of 2-iodoxybenzoic acid increases the yield for these otherwise low yielding condensation reactions between **TAB** and 1,2-diketones. Synthesis of 5 and 10 substituted PQ derivatives follows our

[a]*School of Materials Science and Engineering, Nanyang Technological University, 50 Nanyang Avenue, Singapore, 63979, Singapore. E-mail: hbsu@ntu.edu.sg; Tel: +65 6790 4346*
[b]*Energy Research Institute @NTU (ERI@N), Nanyang Technological University, 50 Nanyang Drive, Singapore, 637553, Singapore. E-mail: ACGrimsdale@ntu.edu.sg; Tel: +65 6790 6728*

† Electronic supplementary information (ESI) available: Characterization including NMR, MALDI-TOF, TGA and DSC. Includes additional DFT information. See DOI: 10.1039/c1jm12347e

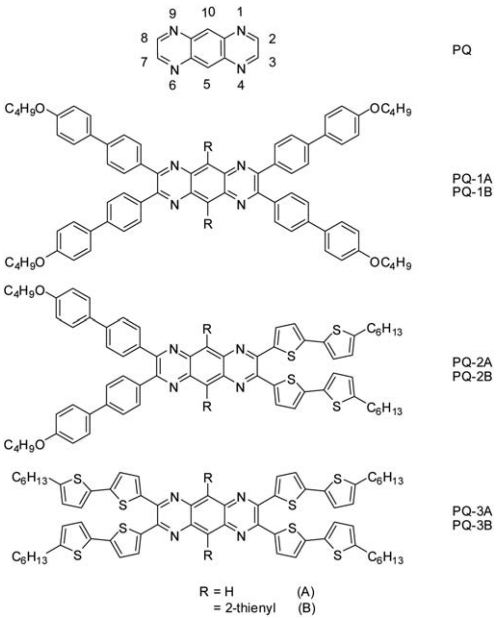


**Fig. 1** Structure of PQ, its IUPAC numbering system and the derivatives discussed in this paper. **PQ-1B** and **PQ-3B** were previously synthesized by us.[17]

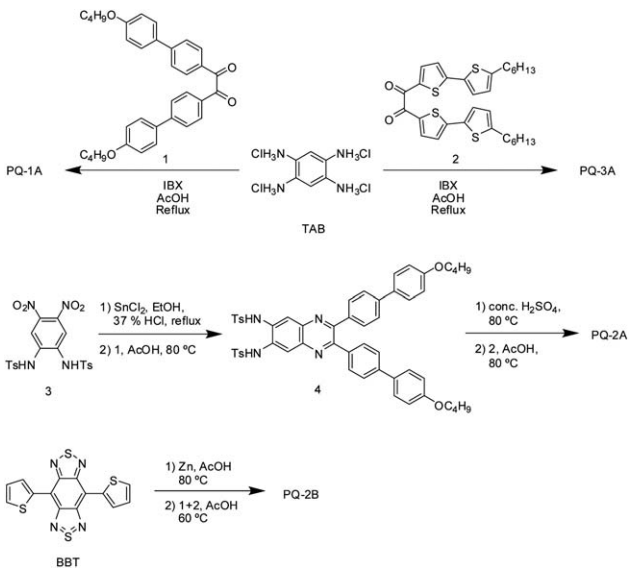


**Scheme 1** Synthesis of the PQ molecules.

previously reported methodology starting from 4,8-dibromo-BBT.[17,20] Reduction of the BBT precursor using zinc in acetic acid, followed by addition of the diketone(s) yielded **PQ-1B**, **PQ-2B** and **PQ-3B**. Synthesis of **PQ-2A** starts with reduction of dinitroditosylaminobenzene **3**, which is prepared according to the literature,[21] using tin(II) in 37% HCl, followed by condensation with the diketone 1. Subsequent deprotection of the tosyl group *via* concentrated sulfuric acid, followed by condensation with diketone 2 yielded **PQ-2A**.

### Comparison of experimental and theoretical results

From Table 1, an increase in conjugation from biphenyl to bithienyl with the PQ core results in the band gap reduction of the molecules in series A. The subsequent addition of quinodal thienyls reduces the band gap further. However, this reduction in band gap from series A to B decreases from changing biphenyls to bithienyls (**PQ-1A** → **PQ-1B** > **PQ-2A** → **PQ-2B** > **PQ-3A** → **PQ-3B**). We suspect that this decrease in reduction of the band gap might be a consequence of cross-conjugation between the arms and the quinoidal positions. To confirm this, the proton shifts of the quinoidal hydrogens in series A were compared (Table 2). The PQ with the strongest quinoid character will have the most deshielded quinoidal hydrogens and thus these will show up at the most down-field position in the $^1$H NMR spectrum.[22] From the proton shift of series A, we can see that the strength of the quinoid character is **PQ-1A** > **PQ-2A** > **PQ-3A**. The progressive weakening of the quinoid character according to the proton shift in the series can be attributed to a cross-conjugation effect caused by the addition of aromatic arms with increasing electron donating nature. Scheme 2 shows the resonance structures depicting conjugation and cross-conjugation between the arm and quinodal positions within the PQ core. Decreasing the quinoid character would mean that the proton shift in series B would follow the trend: **PQ-1B** > **PQ-2B** > **PQ-3B**, which is in agreement with the observed results.

Computational modeling results are tabulated in Table 3. The theoretical trends of the HOMO match those of the experimental data. As expected, series A shows a major HOMO contribution from the arm position while series B shows higher HOMO electron density along the quinoidal positions and core due to the high quinoid character at these positions.[4–8] For series A, both theoretical and experimental HOMO values increase due to the stronger electron-donating nature of bithienyl as compared to biphenyl. The HOMO (HOMO − 1) orbitals show two nodes existing in the PQ core, in **PQ-1A** (**PQ-1B**) and **PQ-3A** (**PQ-3B**) at the center carbons bearing the hydrogen and in **PQ-2A** (**PQ-2B**) at the two nitrogens nearer to the biphenyl arms. Cross-conjugation has been reported to produce destructive quantum interference (node) in molecular electronics.[23–25] In Table 4, tetramethyl substituted molecules of series A (PQ-0A) and B (PQ-0B) show the absence of nodes in their HOMO and HOMO − 1. Thus the origin of these nodes in **PQ-1A** → **PQ-3A** and **PQ-1B** → **PQ-3B** must be a result of cross-conjugation of the aromatic arm substituents. With reference to the resonance structure j in Scheme 2, it becomes intuitive that the contribution from two arm substituents on the same side (quinoid positions as reference line) will result in cross-conjugation with another two on the other side.

From series A to B, the increase in both theoretical and experimental HOMO levels can be thought of as the formation of a new set of bonding orbitals from the addition of the thienyl substitutions at the quinoidal positions, which is localized along the quinoid–core–quinoid system. Within series B, both theoretical and experimental HOMO values are almost constant, with a slight stabilization from **PQ-1B** to **PQ-3B**. This slight stabilization can be thought as the HOMO being slightly more delocalized due to the contribution from bithienyls, a case of pseudo-cross-conjugation as suggested by five resonance structures (d, e, h, i and j in Scheme 2) that show conjugation between quinoidal and arm positions.

The theoretical trend of LUMO energy levels for series B agrees nicely with the experimental data. However, the

**Table 1** Characterization of PQ molecules[a]

| | HOMO/eV | LUMO/eV | $E_{g\ (CV)}$/eV | $E_{g\ (UV)}$/eV | $\lambda_{max}$/nm solution | $T_m$/°C |
|---|---|---|---|---|---|---|
| **PQ-1A** | −5.91 | −3.66 | 2.25 | 2.48 | 454, 339s, 304 | >300 |
| **PQ-1B** | −5.10 | −3.12 | 1.98 | 1.93 | 543t, 490, 382, 324 | >300 |
| **PQ-2A** | −5.82 | −3.61 | 2.21 | 2.16 | 499, 361s, 301 | 211 |
| **PQ-2B** | −5.14 | −3.14 | 2.00 | 1.96 | 541, 409, 324 | 132 |
| **PQ-3A** | −5.49 | −3.55 | 1.94 | 1.98 | 573, 550, 387, 331 | 191 |
| **PQ-3B** | −5.15 | −3.26 | 1.89 | 1.86 | 607, 575s, 447, 339 | 170 |

[a] HOMO and LUMO were calculated from cyclic voltammetry. s/t denotes position of shoulder/tail in UV-vis absorption spectra.

**Table 2** Proton shift of the quinoid position hydrogens

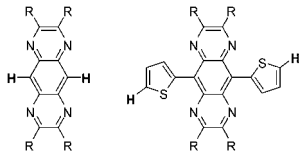

A B

| | PQ-1A | PQ-1B | PQ-2A | PQ-2B | PQ-3A | PQ-3B |
|---|---|---|---|---|---|---|
| H shift/ppm | 9.07 | 8.52 | 8.81 | 8.44 | 8.57 | 8.37 |

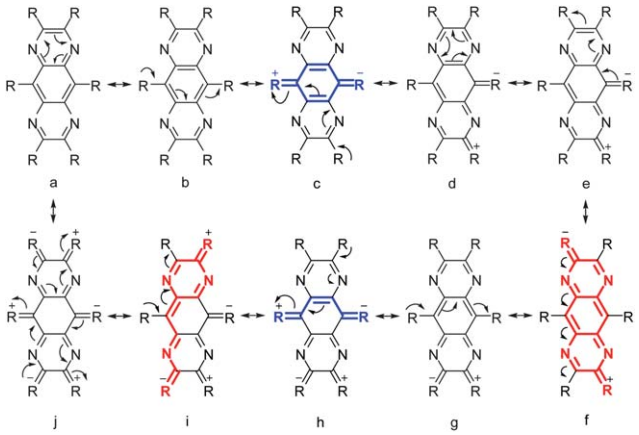

**Scheme 2** Resonance structures illustrating conjugation and cross-conjugation effects between the quinoidal and arm positions. Blue denotes conjugation along the quinoidal positions and red denotes conjugation along the arm positions.

experimental LUMO values within series A and from series A → B increase but the reverse was observed in the calculations. Only the experimental and theoretical LUMO trends for series B match. The discrepancies may arise from the possible agglomeration in the cyclic voltammetry experiment as compared to the single molecule gas phase used in the computational studies. More detailed studies on the discrepancies are currently underway. Here we focus on the understanding from theoretical results. For series A, the LUMO gets more delocalization from 1A to 3A, thus lower energy values. Addition of the thienyls at the quinoidal positions for series B results in a more delocalized LUMO as compared to series A. Thus the LUMOs of series B are lower than those of series A. Within series B, the LUMO also gets more delocalization from 1B to 3B, thus lower energy values. However, the decrease is of a smaller magnitude as compared to series A. This is because the pseudo-cross-conjugation discussed earlier only induces a little more delocalization of the LUMO in series B.

## Photophysical properties

In the theoretical calculation, the vertical absorptions and UV-vis spectrum were calculated by the TD-DFT approach with the 6-31G(d) basis set. 20 states were calculated. The calculated dipole-allowed absorptions associated with the oscillator strengths and the assignments are listed in Table 5, and the simulated Gaussian type absorption spectra (the UV-vis peak half-width at half height is 0.15 eV) are shown in Fig. 2a. The electron excitation from the HOMO to the LUMO corresponds to the π–π* type transition between donor and acceptor moieties. Interestingly, the lowest-lying absorptions are red-shifted from series A to series B, and the red-shifts also exist within each series (from biphenyl to bithienyl substitutions). The overall absorption band measured by experiment can be described by the calculated spectra broadened with a Gaussian function. The first absorption bands of series A are all attributed to the HOMO → LUMO transition and their oscillator strengths are quite strong, ranging from 0.9225 to 1.0321. In contrast, the HOMO → LUMO transitions for series B have very weak oscillator strength, ranging from 0.0135 to 0.1033. For series B, only the HOMO → LUMO transition for **PQ-1B** is observable. This is because the next absorption band for **PQ-1B**, which is attributed to the HOMO − 1 → LUMO transition, is much higher in energy (>1 eV difference) than its HOMO → LUMO transition. For **PQ-2B** and **PQ-3B**, the next absorption bands, which are also attributed to the HOMO − 1 → LUMO transition, have much higher oscillator strength than their HOMO → LUMO transition and both bands are similar in energy (<0.25 eV difference). The combination of the two effects causes the HOMO → LUMO transition for both **PQ-2B** and **PQ-3B** to be not observable after spectra broadening.

For the experimental absorption spectra measured in solution, the lowest-lying absorptions are also red shifted from series A to series B, and the red-shifts also exist within each series (from biphenyl to bithienyl substitutions). This is consistent with the theoretical calculation. The tailing observed in **PQ-1B** is expected to be attributed to the weak HOMO → LUMO transition, as predicted by theoretical calculation.



 

**Table 3** Density functional theory modeling of the PQ molecules using the B3LYP functional and 6-31G* basis set under the geometry optimization condition

| Molecule (symm.) | **PQ-1A** ($D_{2h}$) | **PQ-1B** ($C_2$) | **PQ-2A** ($C_2$) | **PQ-2B** ($C_1$) | **PQ-3A** ($D_{2h}$) | **PQ-3B** ($C_2$) |
|---|---|---|---|---|---|---|
| LUMO + 1/eV/ orbital symm. | 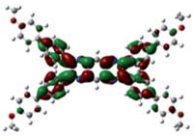 | 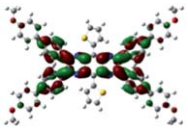 | 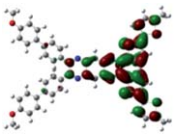 | 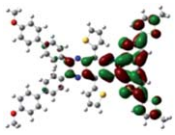 | 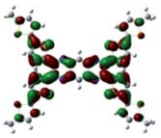 | 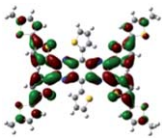 |
| | −1.46/a | −1.48/a | −1.89/a | −1.86/a | −2.00/a | −1.98/a |
| LUMO/eV/orbital symm. | 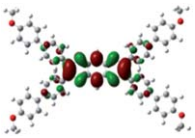 | 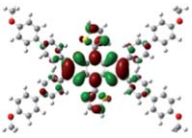 | 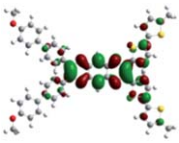 | 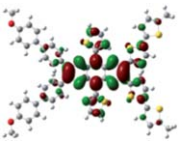 | 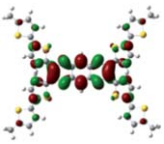 | 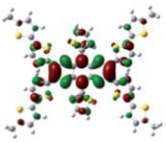 |
| | −2.50/$b_2$ | −2.65/a | −2.60/b | −2.69/a | −2.68/$b_2$ | −2.73/a |
| HOMO/eV/orbital symm. | 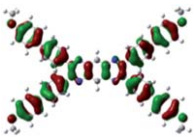 | 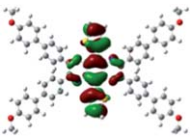 | 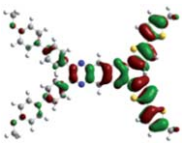 | 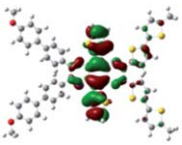 | 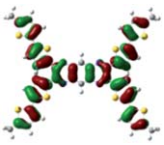 | 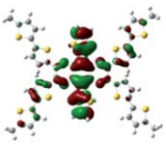 |
| | −5.36/$b_1$ | −4.88/b | −5.15/b | −4.90/a | −5.01/$b_1$ | −4.92/b |
| HOMO − 1/eV/orbital symm. | 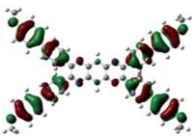 | 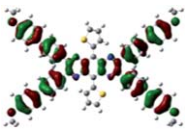 | 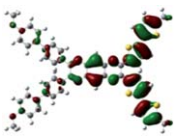 | 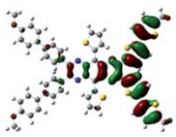 | 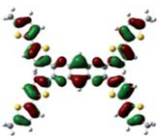 | 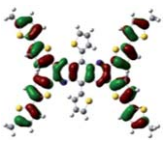 |
| | −5.54/$b_2$ | −5.40/b | −5.40/a | −5.15/a | −5.31/$b_3$ | −5.04/b |

**Table 4** HOMO and HOMO − 1 of the PQ-0A and PQ-0B using the B3LYP functional and 6-31G* basis set under the geometry optimization condition

| | PQ-0A | PQ-0B |
|---|---|---|
| | 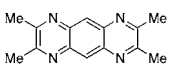 | 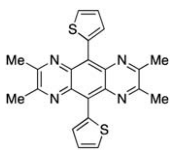 |
| HOMO |  | 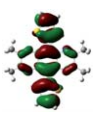 |
| HOMO − 1 |  |  |

**Table 5** Singlet excitation energies, absorption wavelength and their corresponding oscillator strength from TD-B3LYP calculations for the PQ molecules in gas phase

| | $\lambda$/nm | $E_{ex}$/eV | Oscillator | Transition |
|---|---|---|---|---|
| **PQ-1A** | 498 | 2.49 | 0.9425 | HOMO → LUMO |
| | 351 | 3.53 | 0.5875 | HOMO → LUMO + 1 |
| | 337 | 3.68 | 1.9795 | HOMO − 1 → LUMO + 1 |
| **PQ-1B** | 655 | 1.89 | 0.1033 | HOMO → LUMO |
| | 523 | 2.37 | 0.6464 | HOMO − 1 → LUMO |
| | 427 | 2.90 | 0.4830 | HOMO → LUMO + 1 |
| | 365 | 3.40 | 0.7713 | HOMO − 1 → LUMO + 1 |
| **PQ-2A** | 558 | 2.22 | 0.9225 | HOMO → LUMO |
| | 397 | 3.12 | 1.0811 | HOMO − 1 → LUMO + 1 |
| **PQ-2B** | 667 | 1.86 | 0.0431 | HOMO → LUMO |
| | 587 | 2.11 | 0.5759 | HOMO − 1 → LUMO |
| | 476 | 2.61 | 0.6721 | HOMO → LUMO + 1 |
| | 430 | 2.88 | 0.5311 | HOMO − 1 → LUMO + 1 |
| **PQ-3A** | 611 | 2.03 | 1.0321 | HOMO → LUMO |
| | 534 | 2.31 | 0.1698 | HOMO − 1 → LUMO |
| | 426 | 2.91 | 1.3236 | HOMO − 1 → LUMO + 1 |
| **PQ-3B** | 676 | 1.83 | 0.0135 | HOMO → LUMO |
| | 628 | 1.97 | 0.7467 | HOMO − 1 → LUMO |
| | 492 | 2.52 | 0.8852 | HOMO → LUMO + 1 |
| | 456 | 2.72 | 0.8772 | HOMO − 1 → LUMO + 1 |

From both theoretical calculation and experimental results, the lowest-lying intense absorptions for both series A and B correspond very well with each other. As mentioned previously, this absorption band is attributed to the HOMO → LUMO transition for series A and HOMO − 1 → LUMO transition for series B. From the molecular orbitals in Table 3, we can see that the HOMO − 1 and LUMO of series B are very similar in shapes and energies to the HOMO and LUMO of series A, respectively. This striking resemblance thus accounts for the great similarity in the lowest-lying intense absorptions between series A and B.

Using such a strategy to introduce different chromophores in PQ molecules enables broader light absorption. This is proven by the thin film UV-vis absorption shown in Fig. 2c, where the molecules in series B can show strong light absorption up to

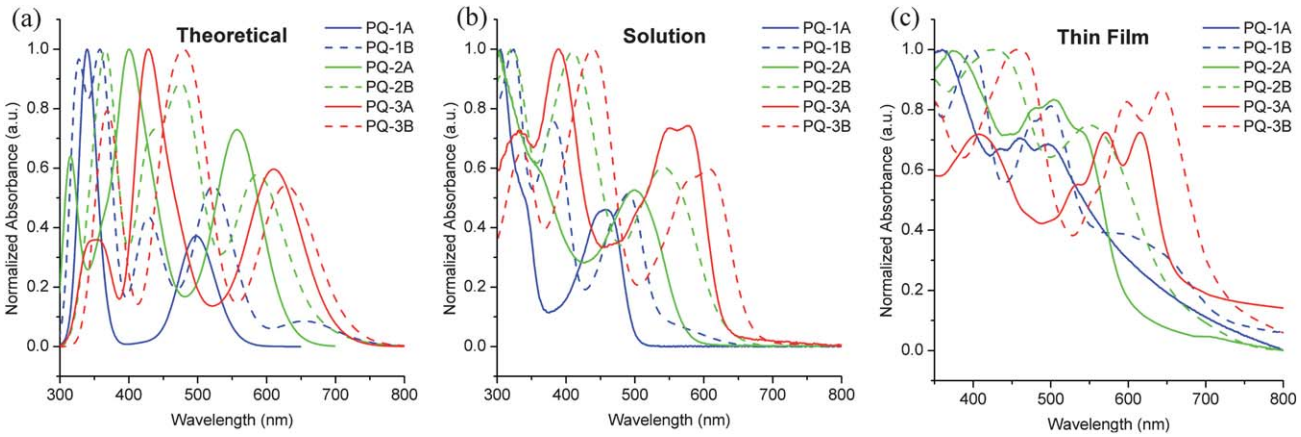


**Fig. 2** The (a) simulated Gaussian type absorption spectra for the PQ molecules in gas phase and experiment in (b) solution and (c) thin film.

~700 nm. Preliminary results suggest that polymerization through the quinoid positions could produce efficient light absorption up to 900 nm. Such broad absorption spectra is one of the criteria for efficient harvesting of solar energy,[26] suggesting such polymers would be very promising materials for organic solar cell applications. Investigations into such polymers are underway and will be published separately.

## Conclusions

In conclusion, we have synthesized and characterized a series of PQ molecules with a systematic change in the substituents. We have observed a series of complex conjugation effects from the arms and substituents at the quinoidal positions, which explains the electronic properties of the PQ molecules. By changing the substituents on the arms, we can achieve strong light absorption up to 700 nm for the small molecules and we believe absorption at even longer wavelengths will be possible for conjugated polymers containing these units. Computational modeling shows agreement with the experimental results in the HOMO trend but fails at times to predict the LUMO, possibly due to agglomeration in the cyclic voltammetry experiment. Nonetheless, this fundamental work allows better understanding of the electronic structures of these systems, which is crucial in designing new materials for organic electronics.

## Experimental section

### Materials

All reagents were purchased from Sigma Aldrich and used without further purification, unless otherwise stated. Column chromatography was carried out with Merck silica-gel (230–400 mesh) while thin layer chromatography (TLC) was performed on Merck silica-gel 60 Al-backed plates (20 cm × 20 cm).

### Characterization

$^1$H data were obtained on a Bruker DPX 400 MHz spectrometer with chemical shifts referenced to $CDCl_3$. Matrix assisted laser desorption/ionization time-of-flight (MALDI-TOF) mass spectra were obtained on a Shimadzu Biotech AXIMA-TOF.[2] Elemental analysis was obtained *via* a Thermo Scientific Flash 2000 Series CHNS/O Analyzer. Differential scanning calorimetry (DSC) was carried out under nitrogen on a DSC Q100 instrument from TA Instruments at a scanning rate of 10 °C min$^{-1}$. 2 cycles were performed, with the 1st cycle from 40 °C to 300 °C to 0 °C and 2nd cycle from 0 °C to 300 °C to 0 °C. Thermogravimetric analysis (TGA) was carried out on a TA Instrument Q500 Thermogravimetric Analyzer at a heating rate of 20 °C min$^{-1}$ up to 900 °C. UV-vis absorption spectra were recorded on a Lambda 900 Spectrometer from Perkin Elmer. Cyclic voltammetry experiments were performed using a multichannel potentiostat (Model 1470E) from Solartron Analytical. All CV measurements were recorded in $CH_2Cl_2$ with 0.1 M tetrabutylammonium hexafluorophosphate as a supporting electrolyte (scan rate of 100 mV s$^{-1}$). The experiments were performed at room temperature with a conventional three electrode configuration consisting of a platinum wire working electrode, a gold counter electrode, and an Ag/AgCl in 3 M KCl reference electrode. The measured potentials were converted to the SCE (saturated calomel electrode with reduction potential of −4.4 eV relative to vacuum).

### Computational methods

Atomistic simulation, using density function theory (DFT) at B3LYP[27,28] (which includes the gradient corrected exchange and correlation functionals along with the exact exchange) method with double-ζ quality basis functions 6-31G* (augmented with polarized function for all non-hydrogen atoms), was used to optimize the geometry of the pyrazino quinoxaline molecules. Geometry was fully relaxed and no symmetry constraints were imposed during optimization using Gaussian 09 code[29] with a convergence criterion of $10^{-3}$ a.u. on the gradient and displacement and $10^{-6}$ a.u. on energy and electron density. Harmonic vibrational analyses showed no imaginary frequency, indicating these structures are a local minimum.

The theoretical UV-vis spectrum was calculated by the time-dependent density functional theory (TD-DFT) approach. All of the calculations were based on 6-31G(d) with Gaussian 09 software package. For each molecule, 20 states are calculated. The calculations are in the gas phase. The calculated dipole-allowed absorptions associated with the oscillator strengths and their assignments are given in Table 5. The simulated Gaussian type

 

absorption spectra (Fig. 2a) are plotted using half-width at half height of 0.15 eV.

## Synthesis

**2,3,7,8-Tetra(4′-butoxy-1′,4-biphen-1-yl)pyrazino[2,3-*g*]quinoxaline (PQ-1A).** 120 mg of **TAB** (0.42 mmol), 471 mg of **1** (0.93 mmol) and 5 mg of IBX (2 mol%) were added to a round bottom flask containing 20 mL of acetic acid. The reaction was refluxed for 2 days. The reaction mixture was poured into water, filtered and the solids were washed with water and ethanol. Column chromatography was carried out using dichloromethane. The resultant yellowish-orange solids were recrystallized using toluene/ethanol to yield yellowish-orange crystals (278 mg, 61% yield). $^1$H NMR ($CDCl_3$): $\delta$ [ppm] 1.00 (t, 12H, $J = 7.2$ Hz), 1.52 (m, 8H), 1.80 (quintet, 8H, $J = 8.0$ Hz), 4.02 (t, 8H, $J = 6.8$), 6.99 (d, 8H, $J = 8.8$ Hz), 7.58 (d, 8H, $J = 8.8$ Hz), 7.61 (d, 8H, $J = 8.4$ Hz), 7.75 (d, 8H, $J = 8.4$ Hz), 9.07 (s, 2H). $^{13}$C NMR ($CDCl_3$): $\delta$ [ppm] 14.0, 19.4, 31.5, 68.0, 115.1, 126.7, 128.3, 128.7, 130.6, 132.6137.2, 142.0, 155.0, 159.3. Anal. Calcd for $C_{74}H_{70}N_4O_4$: C, 82.34; H, 6.54; N, 5.19; O, 5.93. Found: C, 81.84; H, 6.50; N, 5.18. MALDI-TOF-MS *m*/*z*: 1079.44 ($M^+$); calcd. for $C_{74}H_{70}N_4O_4$ = 1079.37.

**2,3-Bis(4′-butoxy-1′,4-biphen-1-yl)-7,8-bis(*p*-toluenesulfonamido)-phenazine (4).** A mixture of compound **3** (0.5 g, 0.99 mmol) and $SnCl_2$ (1.1 g, 5.9 mmol) suspended in a mixture of EtOH (15 mL) and 37% HCl (10 mL) was heated at 85 °C for 3 h. The reaction mixture was cooled down to room temperature and poured into water, neutralized with saturated $NaHCO_3$ solution and extracted with ethyl acetate. The organic layer was collected, dried over anhydrous $MgSO_4$ and filtered. The filtrate was stripped from solvent to obtain yellow solid intermediate which was immediately mixed with **1** (0.45 g, 0.90 mmol) in 20 mL acetic acid and heated to 85 °C for 1 day. Then the reaction mixture was poured into water, and extracted with dichloromethane. The organic layer was washed with saturated $NaHCO_3$ solution, dried over $MgSO_4$ and concentrated *in vacuo*. The crude was purified by column chromatography (hexane/EA = 1/1) to afford orange red solid with overall 70% yield (0.63 g). $^1$H NMR ($CDCl_3$): $\delta$ [ppm] 0.99 (t, 6H, $J = 7.2$ Hz), 1.51 (sextet, 4H, $J = 7.6$), 1.79 (quintet, 4H, $J = 8.0$ Hz), 2.35 (s, 6H), 3.99 (t, 4H, $J = 6.4$ Hz), 6.95 (d, 4H, $J = 8.4$ Hz), 7.23 (d, 4H, $J = 7.6$ Hz), 7.50 (m, 12H), 7.73 (m, 4H), 7.96 (s, 2H). $^{13}$C NMR ($CDCl_3$): $\delta$ [ppm] 14.5, 19.9, 22.3, 32.0, 68.4, 115.5, 123.6, 127.1, 128.4, 130.5, 130.9, 132.9, 133.3, 135.8, 137.2, 139.7, 142.1, 145.2, 154.0, 159.8. Anal. Calcd for $C_{54}H_{52}N_4O_6S_2$: C, 70.72; H, 5.71; N, 6.11; S, 6.99. Found: C, 70.53; H, 5.76; N, 6.29; S, 6.86. MALDI-TOF-MS *m*/*z*: 914.09 ($M^-$ − H); calcd. for $C_{54}H_{52}N_4O_6S_2$ = 917.14.

**2,3-Bis(4′-butoxy-1′,4-biphen-1-yl)-7,8-bis(5′-hexyl-2′,5-bithien-2-yl)pyrazino[2,3-*g*]quinoxaline (PQ-2A).** Compound (**4**) (0.5 g, 0.55 mmol) was added to 10 mL conc. $H_2SO_4$ and heated to 80 °C for 2 h. The reaction mixture was cooled down to room temperature, poured into ice water and filtered. The solid was washed with saturated $NaHCO_3$ solution thoroughly followed by deionized $H_2O$, EtOH and hexane to afford purple red solid intermediate which was immediately mixed with **2** (0.27 g, 0.49 mmol) in 20 mL acetic acid and heated at 85 °C for 3 days. The reaction mixture was cooled down to room temperature, poured into water, and extracted with DCM. The organic layer was washed with saturated $NaHCO_3$ solution, dried over $MgSO_4$ and concentrated *in vacuo*. The crude was purified by column chromatography (hexane/DCM = 1/1) to afford deep red solid with overall 46% yield (0.35 g). $^1$H NMR ($CDCl_3$): $\delta$ [ppm] 0.95 (m, 12H), 1.35 (m, 12H), 1.52 (sextet, 4H, $J = 7.6$ Hz), 1.77 (m, 8H), 2.83 (t, 4H, $J = 7.6$ Hz), 4.01 (t, 4H, $J = 6.4$), 6.75 (d, 2H, $J = 3.6$ Hz), 6.97 (d, 4H, $J = 7.6$ Hz), 7.04 (d, 2H, $J = 4.0$ Hz), 7.17 (d, 2H, $J = 3.2$ Hz), 7.45 (d, 2H, $J = 3.6$ Hz), 7.57 (m, 8H), 7.69 (d, 4H, $J = 7.2$ Hz), 8.81 (s, 2H). $^{13}$C NMR ($CDCl_3$): $\delta$ [ppm] 14.5, 14.7, 19.9, 23.2, 29.4, 30.3, 30.9, 32.0, 32.2, 68.4, 115.5, 123.9, 125.4, 125.8, 127.1, 128.2, 128.8, 129.4, 131.1, 131.5, 132.1, 133.1, 134.8,137.5, 140.1, 140.3, 142.4, 143.4, 147.5, 148.2, 159.8. Anal. Calcd for $C_{70}H_{70}N_4O_2S_4$: C, 74.56; H, 6.26; N, 4.97; S, 11.37. Found: C, 74.40; H, 6.44; N, 5.11; S, 11.15. MALDI-TOF-MS *m*/*z*: 1128.99 ($M^+$); calcd. for $C_{70}H_{70}N_4O_2S_4$ = 1127.59.

**2,3-Bis(4′-butoxy-1′,4-biphen-1-yl)-7,8-bis(5′-hexyl-2′,5-bithien-2-yl)-4,9-bis(thien-2-yl)pyrazino[2,3-*g*]quinoxaline (PQ-2B).** The reduced intermediate (0.2 g, 0.56 mmol) in 20 mL acetic acid prepared from **8** according to our previous studies was transferred without purification *via* syringe to a round bottom flask with a mixture of **1** (0.25 g, 0.50 mmol) and **2** (0.27 g, 0.50 mmol) in 15 mL chloroform under $N_2$. The reaction was stirred at 60 °C for 3 days, cooled down to room temperature and poured into water. Extraction was carried out using dichloromethane. The organic layer was washed with saturated $NaHCO_3$ solution, dried over $MgSO_4$ and concentrated *in vacuo*. The crude was purified by column chromatography (hexane/DCM = 1/1) to afford dark purple solid with overall 15% yield (0.11 g). $^1$H NMR ($CDCl_3$): $\delta$ [ppm] 0.91 (t, 6H, $J = 7.2$ Hz), 1.00 (t, 6H, $J = 7.6$ Hz), 1.35 (m, 12H), 1.52 (m, 4H), 1.77 (m, 8H), 2.84 (t, 4H, $J = 7.6$ Hz), 4.02 (t, 4H, $J = 6.4$), 6.76 (d, 2H, $J = 3.6$ Hz), 6.98 (d, 4H, $J = 8.8$ Hz), 7.05 (d, 2H, $J = 4.0$ Hz), 7.17 (d, 2H, $J = 3.6$ Hz), 7.42 (dd, 2H, $J = 4.0$ & 5.0 Hz), 7.60 (m, 8H), 7.78 (dd, 2H, $J = 5.2$ & 0.8 Hz), 7.93 (d, 4H, $J = 8.4$ Hz), 8.45 (dd, 2H, $J = 4.0$ & 1.2 Hz). $^{13}$C NMR ($CDCl_3$): $\delta$ [ppm] 14.6, 14.8, 20.0, 23.3, 29.5, 31.0, 32.0, 32.3, 68.5, 115.6, 124.0, 125.4, 125.9, 126.9, 127.1, 127.9, 128.8, 130.9, 131.6, 132.3, 133.2, 135.0, 135.1, 136.6, 137.2, 137.5, 140.9, 142.4, 144.0, 145.4, 147.6, 152.5, 159.8. Anal. Calcd for $C_{78}H_{74}N_4O_2S_6$: C, 72.52; H, 5.77; N, 4.34; S, 14.89. Found: C, 72.42; H, 5.89; N, 4.51; S, 14.78. MALDI-TOF-MS *m*/*z*: 1293.68 ($M^+$ + H); calcd. for $C_{78}H_{74}N_4O_2S_6$ = 1291.84.

**2,3,7,8-Tetra(5′-hexyl-2′,5-bithien-2-yl)pyrazino[2,3-*g*]quinoxaline (PQ-3A).** 120 mg of **TAB** (0.43 mmol), 516 mg of **2** (0.93 mmol) and 5 mg of IBX (2 mol%) were added to a round bottom flask with 20 mL of acetic acid. The reaction was refluxed for 2 days. The reaction mixture was poured into water, filtered and the solids were washed with water and ethanol. Column chromatography was carried out using hexane/dichloromethane. The resultant dark purple solids were recrystallized using toluene/ethanol to yield dark purple crystals (298 mg, 60% yield). $^1$H NMR ($CDCl_3$): $\delta$ [ppm] 0.91 (t, 12H, $J = 6.8$ Hz), 1.37 (m, 24H), 1.71 (quintet, 8H, $J = 8.0$ Hz), 2.82 (t, 8H, $J = 7.6$), 6.73 (d, 4H, $J = 3.6$ Hz), 7.02 (d, 4H, $J = 4.0$ Hz), 7.15 (d, 4H, $J = 3.6$ Hz), 7.41 (d, 4H, $J = 3.6$ Hz), 8.57 (s, 2H). $^{13}$C NMR ($CDCl_3$): $\delta$ [ppm] 14.3, 22.8, 28.9, 30.4, 31.7, 123.4, 124.9, 125.3, 127.0, 131.5,

134.4139.8, 140.1, 142.8, 147.0, 147.5. Anal. Calcd for $C_{66}H_{70}N_4S_8$: C, 67.42; H, 6.00; N, 4.76; S, 21.82. Found: C, 69.63; H, 6.05; N, 4.72; S, 21.89. MALDI-TOF-MS *m/z*: 1175.55 ($M^+$); calcd. for $C_{66}H_{70}N_4S_8$ = 1175.81.

## Acknowledgements

This work was supported by Robert Bosch (SEA) Pte Ltd and by A*STAR (SERC grant M 47070020).

## References

1 J. Roncali, *Macromol. Rapid Commun.*, 2007, **28**, 1761–1775.
2 G. Brocks and A. Tol, *J. Phys. Chem.*, 1996, **100**, 1838–1846.
3 A. Ajayaghosh, *Chem. Soc. Rev.*, 2003, **32**, 181–191.
4 C. Kitamura, S. Tanaka and Y. Yamashita, *Chem. Mater.*, 1996, **8**, 570–578.
5 C.-L. Pai, C.-L. Liu, W.-C. Chen and S. A. Jenekhe, *Polymer*, 2006, **47**, 699–708.
6 W.-C. Wu and W.-C. Chen, *J. Polym. Res.*, 2006, **13**, 441–449.
7 Y. Fu, W. Shen and M. Li, *Polymer*, 2008, **49**, 2614–2620.
8 A. P. Zoombelt, M. Fonrodona, M. G. R. Turbiez, M. M. Wienk and R. A. J. Janssen, *J. Mater. Chem.*, 2009, **19**, 5336–5342.
9 Y.-Y. Fang, Y.-M. Guo, M. Du, H. Liu, X.-B. Leng and R.-H. Zhang, *Acta Crystallogr., Sect. E: Struct. Rep. Online*, 2001, **57**, o380–0382.
10 M. Bellizzi, G. Crundwell, M. Zeller, A. D. Hunter and B. McBurney, *Acta Crystallogr., Sect. E: Struct. Rep. Online*, 2006, **62**, o5249–o5251.
11 X. Wang, Y. Zhou, T. Lei, N. Hu, E.-Q. Chen and J. Pei, *Chem. Mater.*, 2010, **22**, 3735–3745.
12 S. Miao, M. D. Smith and U. H. F. Bunz, *Org. Lett.*, 2006, **8**, 757–760.
13 A. Neels and H. Stoeckli-Evans, *Acta Crystallogr., Sect. E: Struct. Rep. Online*, 2006, **62**, o4979–o4980.
14 F. Zhang, J. Bijleveld, E. Perzon, K. Tvingstedt, S. Barrau, O. Inganas and M. R. Andersson, *J. Mater. Chem.*, 2008, **18**, 5468–5474.
15 M. Mastalerz, V. Fischer, C.-Q. Ma, R. A. J. Janssen and P. Bauerle, *Org. Lett.*, 2009, **11**, 4500–4503.
16 E. Wang, L. Hou, Z. Wang, S. Hellstrom, W. Mammo, F. Zhang, O. Inganas and M. R. Andersson, *Org. Lett.*, 2010, **12**, 4470–4473.
17 H. Li, T. L. Tam, Y. M. Lam, S. G. Mhaisalkar and A. C. Grimsdale, *Org. Lett.*, 2011, **13**, 46–49.
18 F. De Proft and P. Geerlings, *Chem. Rev.*, 2001, **101**, 1451–1464.
19 H. Wang, Y. Wen, X. Yang, Y. Wang, W. Zhou, S. Zhang, X. Zhan, Y. Liu, Z. Shuai and D. Zhu, *ACS Appl. Mater. Interfaces*, 2009, **1**, 1122–1129.
20 T. L. Tam, H. Li, F. Wei, K. J. Tan, C. Kloc, Y. M. Lam, S. G. Mhaisalkar and A. C. Grimsdale, *Org. Lett.*, 2010, **12**, 3340–3343.
21 G. W. H. Cheeseman, *J. Chem. Soc.*, 1962, 1170–1176.
22 M. Kikuchi, H. Kurosu and I. Ando, *J. Mol. Struct.*, 1992, **269**, 183–195.
23 D. Q. Andrews, G. C. Solomon, R. H. Goldsmith, T. Hansen, M. R. Wasielewski, R. P. V. Duyne and M. A. Ratner, *J. Phys. Chem. C*, 2008, **112**, 16991–16998.
24 T. Markussen, R. Stadler and K. S. Thygesen, *Nano Lett.*, 2010, **10**, 4260–4265.
25 G. C. Solomon, D. Q. Andrews, R. H. Goldsmith, T. Hansen, M. R. Wasielewski, R. P. V. Duyne and M. A. Ratner, *J. Am. Chem. Soc.*, 2008, **130**, 17301–17308.
26 X. Wang, E. Perzon, J. L. Delgado, P. D. L. Cruz, F. Zhang, F. Langa, M. Andersson and O. Inganäs, *Appl. Phys. Lett.*, 2004, **85**, 5081–5083.
27 A. D. Becke, *J. Chem. Phys.*, 1993, **98**, 5648.
28 C. Lee, W. Yang and R. G. Parr, *Phys. Rev. B*, 1988, **37**, 785.
29 M. J. Frisch, G. W. Trucks, H. B. Schlegel, G. E. Scuseria, M. A. Robb, J. R. Cheeseman, G. Scalmani, V. Barone, B. Mennucci, G. A. Petersson, H. Nakatsuji, M. Caricato, X. Li, H. P. Hratchian, A. F. Izmaylov, J. Bloino, G. Zheng, J. L. Sonnenberg, M. Hada, M. Ehara, K. Toyota, R. Fukuda, J. Hasegawa, M. Ishida, T. Nakajima, Y. Honda, O. Kitao, H. Nakai, T. Vreven, J. A. Montgomery, Jr., J. E. Peralta, F. Ogliaro, M. Bearpark, J. J. Heyd, E. Brothers, K. N. Kudin, V. N. Staroverov, R. Kobayashi, J. Normand, K. Raghavachari, A. Rendell, J. C. Burant, S. S. Iyengar, J. Tomasi, M. Cossi, N. Rega, J. M. Millam, M. Klene, J. E. Knox, J. B. Cross, V. Bakken, C. Adamo, J. Jaramillo, R. Gomperts, R. E. Stratmann, O. Yazyev, A. J. Austin, R. Cammi, C. Pomelli, J. W. Ochterski, R. L. Martin, K. Morokuma, V. G. Zakrzewski, G. A. Voth, P. Salvador, J. J. Dannenberg, S. Dapprich, A. D. Daniels, Ö. Farkas, J. B. Foresman, J. V. Ortiz, J. Cioslowski and D. J. Fox, *Gaussian 09 Revision*, Gaussian, Inc., Wallingford CT, 2009.

 